Pramāṇa, Vol. 23, No. 6, December 1984, pp. 767–783. © Printed in India.

Light ion fusion in deformation model

R C NAYAK*
Institute of Physics, Bhubaneswar 751 005, India
Present Address: S. V. M. College, Jagatsinghpur, Cuttack 754 103, India

MS received 28 December 1983; revised 12 July 1984

Abstract. Experiments with heavy ions at moderate energies show the importance of deformation in heavy ion collisions. A deformation model which takes deformation dynamically into account is developed. Having described fusion and deep inelastic collision for a very heavy system (Xe + Bi) and a medium heavy system (Ar + Th) at various energies successfully, we turn to some comparatively lighter heavy ions where fusion is the most dominant feature. Fusion cross-sections for six pairs of lighter systems ($^{35}Cl + ^{116}Sn$, $^{58}Ni + ^{62}Ni$, $^{35}Cl + ^{62}Ni$, $^{32}S + ^{24}Mg$, $^{24}Mg + ^{24}Mg$ and $^{12}C + ^{27}Al$) have been obtained using our deformation model which agree well with experiment. The two-slope-behaviour of fusion excitation function which is an important feature of light ion fusion systematics is also obtained, in our model calculations for all the systems studied.

Keywords. Fusion excitation function; deformation; two-slope-behaviour; folding potential; critical radius; deep inelastic collision.

PACS No. 34·10-x

1. Introduction

In the last decade, experiments have been conducted using heavy systems like Ar + Th, Kr + Bi and Xe + Bi at moderate energies in which very low energy reaction products with energies much below the spherical coulomb barrier have been detected. This shows the importance of deformation in the dynamics of heavy ion collisions. The spherical model of Gross *et al* (1974) was qualitatively successful in explaining heavy ion collision data but it gave too high fusion cross-sections and too low energy loss. Inclusion of phenomenological deformation by Wilczynska and Wilczynski (1976) improves energy loss but worsens fusion cross-section. The relative success and shortcomings of the above models prompted us (Gross *et al* 1981) to develop a dynamical model in which deformation is treated as a new generalised co-ordinate of the system. This deformation model (Gross *et al* 1981) circumvents the difficulties encountered in the spherical model (Gross *et al* 1974) and the phenomenological deformation model (Wilczynska and Wilczynski 1976) and is able to describe deep inelastic collision (DIC) and fusion processes satisfactorily in heavy systems like Ar + Th and Xe + Bi at various energies. The friction and potential parameters of spherical model of Gross *et al* (1974) have been retained in our deformation model.

Earlier we (Nayak 1983) have successfully described the fusion and DIC of a very heavy system (Xe + Bi at E_{lab} = 700, 940, 1130 and 1422 MeV) and a medium heavy system (Ar + Th at E_{lab} = 220, 250, 379, 500, 700 MeV). In this paper we apply our model to some comparatively lighter ions ($^{35}Cl + ^{116}Sn$, $^{58}Ni + ^{62}Ni$, $^{35}Cl + ^{62}Ni$, ^{32}S

$+^{24}$Mg, ^{24}Mg$+^{24}$Mg and ^{12}C$+^{27}$Al) some of which have been studied rather recently. In §2 we present the theory of our model in detail. Section 3 gives the results of our calculation and §4 a brief conclusion.

2. Theory

The geometry of the two colliding nuclei adopted in our deformation model is presented in figure 1. We describe the total system by the collective co-ordinates r, θ and α where $r = |\mathbf{r}|$ is the distance between the centres of the interacting nuclei, θ is the polar angle of $\mathbf{r}$ and α is the spheroidal deformation defined as the ratio of the semi axes perpendicular and parallel to the symmetry axis which is taken to be the line connecting the two centres of the nuclei. To keep the dynamics simple and tractable, we assume that throughout the process of interaction, nose-to-nose symmetry is maintained. This means the symmetry axis is coincident with the major axes of the two colliding nuclei. We assume that at any instant the deformations of the two nuclei are identical. Thus prolate, spherical and oblate shapes of the nuclei are described by different values of α as: $\alpha < 1$ prolate, $\alpha = 1$ sphere, and $\alpha > 1$ oblate. Thus the deformation of both the nuclei are described by one co-ordinate α. This is of course a serious over-simplification. Allowing for different deformations α_1 and α_2 for the two nuclei demands the calculation of nuclear potential $V_N(r, \alpha_1, \alpha_2)$ in three-dimensional parameter space. This was not possible technically. The restriction to coinciding symmetry axes (collinear symmetry axes) may not be a serious simplification because the frictional coupling is very strong and forces the two shapes to follow one another.

2.1 *Equations of motion*

The system is described by the lagrangian

$$L = T - V,$$

where the kinetic energy T and potential energy V are given as

$$T = \tfrac{1}{2}\mu\dot{r}^2 + \tfrac{1}{2}\mu r^2\dot{\theta}^2 + \tfrac{1}{2}\mu(\alpha)\dot{\alpha}^2,$$

and

$$V = V_1(\alpha) + V_2(\alpha) + V_{ic}(\alpha, r) + V_N(\alpha, r). \tag{1}$$

Here $\mu = A_1A_2/(A_1 + A_2)$ is the reduced mass of the system and V_i the self-energies of the nuclei 1 and 2, $V_{ic}(\alpha, r)$ the coulomb interaction energy between the nuclei with deformation α when the two centres of mass are at a distance r, $V_N(\alpha, r)$ the nuclear

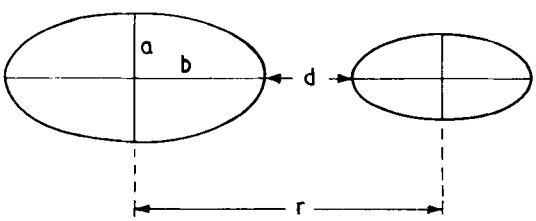

Figure 1. Geometry of two colliding spheroidal nuclei.

interaction energy at deformation α and separation r and $\mu(\alpha)$ is the vibrational mass parameter or the mass associated with the deformation degree of freedom.

For dissipative forces we take radial, tangential and vibrational friction. However, unlike in the spherical model we assume that the radial friction force is proportional to the relative velocity of the surface $\dot{d}$ rather than the velocity of the centres of mass $\dot{r}$. We call this as the surface friction. The separating distance d between the two surfaces when the nuclei are spherical with their centres at a distance r apart is given as

$$d = r - (R_1 + R_2),$$

and the surface separation d for identical deformation α is given as

$$d = r - (b_1 + b_2) = r - (R_1 + R_2)/\alpha^{2/3}. \tag{2}$$

Here R_i are the equivalent sharp radii of the spherical nuclei and b_i the semi major axes of the deformed nuclei. From volume conservation $b_i = R_i/\alpha^{2/3}$. From (2)

$$\partial d/\partial\alpha = (2/3)(R_1 + R_2)\alpha^{-5/3},$$

and

$$\dot{d} = \dot{r} + \frac{\partial d}{\partial \alpha}\dot{\alpha}. \tag{3}$$

So $\dot{r} = 0$, does not imply $\dot{d} = 0$. Thus our friction force has a simple physical meaning. When the two nuclei are in contact and the relative velocity $\dot{r} = 0$, the vibration of the shape still continues to give rise to friction. Hence we take the radial friction to be proportional to $\dot{d}$, the tangential friction proportional to $r\dot{\theta}$ and the vibrational friction describing the damping of the isolated nuclei proportional to $\dot{\alpha}$. Thus the Raleigh dissipation function

$$\mathscr{R} = \tfrac{1}{2} K_r \dot{d}^2 + \tfrac{1}{2} K_\theta r^2 \dot{\theta}^2 + \tfrac{1}{2} K_\alpha \dot{\alpha}^2, \tag{4}$$

where K_r, K_θ and K_α are radial, tangential and vibrational friction coefficients respectively. From the general form of the Lagrangian equation

$$\frac{\mathrm{d}}{\mathrm{d}t}\frac{\partial L}{\partial \dot{q}} - \frac{\partial L}{\partial q} + \frac{\partial \mathscr{R}}{\partial \dot{q}} = 0,$$

we can get the respective equations in the three degrees of freedom r, θ and α. Thus the radial equation is

$$\frac{\mathrm{d}}{\mathrm{d}t}\frac{\partial L}{\partial \dot{r}} - \frac{\partial L}{\partial r} + \frac{\partial \mathscr{R}}{\partial \dot{r}} = 0.$$

Using (3) and (4) the radial equation becomes

$$\mu\ddot{r} - \mu r\dot{\theta}^2 + \frac{\partial}{\partial r}[V_{ic}(\alpha, r) + V_N(\alpha, r)] + K_r\left(\dot{r} + \frac{\partial d}{\partial \alpha}\dot{\alpha}\right) = 0. \tag{5}$$

Similarly from $\dfrac{\mathrm{d}}{\mathrm{d}t}\dfrac{\partial L}{\partial \dot{\theta}} - \dfrac{\partial L}{\partial \theta} + \dfrac{\partial \mathscr{R}}{\partial \dot{\theta}} = 0$, we get

$$\mu r^2\ddot{\theta} + 2\mu r\dot{r}\dot{\theta} + K_\theta r^2\dot{\theta} = 0. \tag{6}$$

Using $\dfrac{\mathrm{d}}{\mathrm{d}t}\dfrac{\partial L}{\partial \dot{\alpha}} - \dfrac{\partial L}{\partial \alpha} + \dfrac{\partial \mathscr{R}}{\partial \dot{\alpha}} = 0$ and (3), we get α degree equations as

$$\mu(\alpha)\ddot{\alpha}+\frac{1}{2}\frac{\partial\mu(\alpha)}{\partial\alpha}\dot{\alpha}^2+\frac{\partial}{\partial\alpha}[V_N(\alpha,r)+V_{ic}(\alpha,r)+V_1(\alpha)+V_2(\alpha)]$$
$$+K_r\left[\dot{r}+\frac{\partial d}{\partial\alpha}+\dot{\alpha}\left(\frac{\partial d}{\partial\alpha}\right)^2\right]+K_\alpha\dot{\alpha}=0. \tag{7}$$

Here the vibrational mass $\mu(\alpha)$ of the two nuclei is the sum of the individual vibrational masses $\mu_1(\alpha)$ and $\mu_2(\alpha)$. For spheroidal deformation α of a nucleus of mass M_i and sharp radius R_i, the vibrational mass $\mu_i(\alpha)$ is given by Nix (1964) as

$$\mu_i(\alpha)=\left(1+\frac{\alpha^2}{2}\right)M_iR_i^2/5. \tag{8}$$

We take the radial and tangential friction form factors as used by Gross *et al* (1974) in the spherical model as

$$K_r=K_r^0\left[\frac{\partial V_N(\alpha,r)}{\partial r}\right]^2,$$
and
$$K_\theta=K_\theta^0\left[\frac{\partial V_N(\alpha,r)}{\partial r}\right]^2, \tag{9}$$

with the same strengths of friction coefficients

$$K_r^0=0{\cdot}4\times10^{-22}\ \text{sec/MeV},$$
$$K_\theta^0=0{\cdot}001\times10^{-22}\ \text{sec/MeV}. \tag{10}$$

For vibrational friction coefficient K_α we use the expression (Deubler and Dietrich 1977)

$$K_\alpha=(16/9)\pi\eta(R_1^3+R_2^3), \tag{11}$$

where η is the viscosity coefficient. We took $\eta=1\times10^{-22}$ MeV sec/fm^3.

2.2 *Nuclear potential*

To calculate the nuclear interaction potential in the spherical model, the single folding method was used where the interaction energy between two ions 1 and 2 with their centres of mass at a distance r is given as

$$V_N^{12}(r)=\int\rho_1(r_1)V_2(|\mathbf{r}-\mathbf{r}_1|)\,\mathrm{d}^3r_1. \tag{12}$$

Here the nucleus-nucleon potential V_2 between nucleus 2 and a nucleon is folded into the density distribution ρ_1 of nucleus 1 at the position of the nucleon at a distance r_1 from the centre of nucleus 1. In the spherical model the nucleus-nucleon potential and density distributions are diffuse surfaces and the two interacting nuclei are spherical in shape. In our deformation model we follow the same procedure but the interaction energy is calculated for two spheroidally deformed nuclei where deformation $\alpha=1$ yields the spherical model result. In our model these distributions are not only functions of separation but also of deformation α of the nuclei.

Taking an elliptical cross-section of a spheroid of deformation α, any radius vector r in general is

$$r = \frac{a_i}{\left[1-\left(1-\frac{a_i^2}{b_i^2}\right)\cos^2\psi\right]^{1/2}} = \frac{a_i}{[1-(1-\alpha^2)\cos^2\psi]^{1/2}}, \tag{13}$$

where ψ is the angle that r makes with the semi major axis b_i. Here a_i is the semi minor axis and deformation $\alpha = \alpha_i/b_i$. Now the potential and the density distribution as functions of deformation α and angle ψ is

$$V_2(|\mathbf{r}-\mathbf{r}_1|, \alpha) = \frac{V_0}{1+\exp\left(\frac{|\mathbf{r}-\mathbf{r}_1| - R_{2P}(\alpha,\psi)}{a_P}\right)},$$

and

$$\rho_1(r_1, \alpha) = \frac{\rho_0}{1+\exp\left(\frac{r_1 - R_{1D}(\alpha,\psi)}{a_D}\right)}, \tag{14}$$

where the half radius R_{2P} for potential and R_{1D} for density distribution are functions of α and ψ (using (13))

$$R_{2P}(\alpha,\psi) = \frac{a_{2P}}{[1-(1-\alpha^2)\cos^2\psi_P]^{1/2}},$$

and

$$R_{1D}(\alpha,\psi) = \frac{a_{1D}}{[1-(1-\alpha^2)\cos^2\psi_D]^{1/2}}. \tag{15}$$

Here ψ_P and ψ_D are the angles for potential and density distribution respectively. Potential V_2 and density distribution ρ_1 are taken in the fermi distribution form and do not have sharp boundaries; a_P, a_D are diffuseness coefficients for potential and density distribution respectively, V_0 is the strength of the nuclear potential and ρ_0 is the central density. We have taken the following parameters used by Gross *et al* (1974)

$$V_0 = -50 \text{ MeV}; \quad \rho_0 = 0{\cdot}17/\text{fm}^3; \quad a_P = 0{\cdot}65 \text{ fm} \quad a_D = 0{\cdot}54 \text{ fm};$$
$$R_{iP}^0 = 1{\cdot}25\, A_i^{1/3} \text{ fm}; \quad R_{iD}^0 = 1{\cdot}12\, A_i^{1/3} - 0{\cdot}86\, A_i^{-1/3} \text{ fm}.$$

Here $R_{iP,D}^0$ refer to the spherical nuclei. The semi axes of the deformed nuclei can be expressed in terms of radii of equivalent spheres. Thus from volume conservation, the semi axes a_i and b_i for potential and density are

$$a_{iP,D} = R_{iP,D}^0 \alpha^{1/3},$$
$$b_{iP,D} = R_{iP,D}^0/\alpha^{2/3}.$$

For two spheroidally-deformed nuclei of deformation α centres separated by a distance r, the single folding potential is

$$V_N^{12}(r,\alpha) = \int V_2(|\mathbf{r}-\mathbf{r}_1|, \alpha)\rho_1(r_1,\alpha)\,\mathrm{d}^3 r_1. \tag{16}$$

But $V_N^{12}(r,\alpha) \neq V_N^{21}(r,\alpha)$. Therefore a symmetrised form of the potential is used in our calculation taking the average potential as

$$V_N(r,\alpha) = \frac{V_N^{12}(r,\alpha) + V_N^{21}(r,\alpha)}{2}. \tag{17}$$

The potential is calculated numerically using cylindrical co-ordinates.

2.3 *Coulomb interaction energy*

In the spherical model coulomb interaction energy of two interacting spherical nuclei is given as $Z_1 Z_2 e^2/r$. But this point charge approximation is not valid for spheroidally deformed nuclei. Interaction coulomb energy between two spheroidally deformed nuclei is given in detail by Hirschfelder *et al* (1954) and Nix (1964). It is obvious that this interaction will be dependent on deformation α and r, the distance between the charge centres.

The interaction coulomb energy of two separated charge distributions is given as a multipole summation. Assuming that the symmetry axes of the two charge distributions are coplanar and collinear, a very simplified expression results. The interaction coulomb energy of the two deformed drops as a function of r and α is

$$V_{ic}(\alpha, r) = (Z_1 Z_2 e^2/r)(S_1 + S_2 - 1 + S), \tag{18}$$

where

$$S_{1,2}(\lambda, 0) = 0{\cdot}75\left(\frac{1}{\lambda} - \frac{1}{\lambda^3}\right)\log\left(\frac{1+\lambda}{1-\lambda}\right) + \frac{3}{2\lambda^2} \quad \text{for prolate}$$

$$S_{1,2}(w, 0) = 1{\cdot}5\left(\frac{1}{w} + \frac{1}{w^3}\right)\tan^{-1} w - \frac{3}{2w^2} \quad \text{for oblate.}$$

Here $\lambda^2 = (b^2 - a^2)/r^2$; b the semi major axis of the prolate drop; a the semi minor axis of the prolate drop and r the separating distance between centres of charge distribution. For the oblate case $w^2 = -\lambda^2$; subscripts 1 and 2 in $S_{1,2}$ refer to nucleus 1 and nucleus 2.

S in (18) for two interacting prolate charge distributions is

$$S = \sum_{j=1}^{\infty}\sum_{k=1}^{\infty} \frac{3}{(2j+1)(2j+3)} \times \frac{3}{(2k+1)(2k+3)} \times \frac{(2j+2k)!}{2j!\,2k!} \lambda_1^{2j} \lambda_2^{2k}, \tag{19}$$

and for oblate charge drops

$$S = \sum_{j=1}^{\infty}\sum_{k=1}^{\infty} \frac{3}{(2j+1)(2j+3)} \times \frac{3}{(2k+1)(2k+3)} \times \frac{(2j+2k)!}{2j!\,2k!} (-1)^{j+k} w_1^{2j} w_2^{2k}. \tag{20}$$

λ_1, λ_2 refer to nucleus 1 and 2 respectively. For prolates

$$\lambda_i^2 = (b_i^2 - a_i^2)/r^2 = b_i^2(1 - \alpha^2)/r^2$$

and

$$\alpha = \frac{a_i}{b_i} = \frac{\text{semi axis perpendicular to the symmetry axis}}{\text{semi axis parallel to the symmetry axis}}.$$

For oblates $w_i^2 = -\lambda_i^2 = (a_i^2 - b_i^2)/r^2 = b_i^2(\alpha^2 - 1)/r^2$. For oblates $a_i > b_i$ and hence deformation $\alpha > 1$. For prolates $a_i < b_i$ and hence deformation $\alpha < 1$. For spheres $a_i = b_i$ and hence deformation $\alpha = 1$.

In actual calculation we find that $\sum_{j=1}^{\infty}\sum_{k=1}^{\infty}$ can be taken care of by limiting j and k up to 5. For $\frac{\partial}{\partial r} V_{ic}(\alpha, r)$ and $\frac{\partial}{\partial \alpha} V_{ic}(\alpha, r)$ we have taken the derivatives for appropriate

shapes in our calculation for two interacting spheres $S_1 = S_2 = 1$. For interacting spheres as seen from (19) $\lambda_i = 0$ and hence $S = 0$. So interaction coulomb energy of the two spheres from (18) simplifies to

$$V_{ic}(\alpha = 1, r) = Z_1 Z_2 e^2/r$$

which is a very familiar expression of point charge approximation. Equation (18) presents a rather general and simple expression for coulomb interaction of two spheroidally deformed charge-drops maintaining nose-to-nose symmetry.

2.4 *Self energies*

For our purpose the self energies of the projectile and target will only consist of coulomb and surface terms which are only shape dependent. So $V_1(\alpha)$, $V_2(\alpha)$ used in (1) can be written as

$$V_1(\alpha) = V_1^{\text{CSE}}(\alpha) + V_1^{\text{SSE}}(\alpha),$$

where CSE means coulomb self-energy and SSE means surface self-energy. For spheroidal deformation α these quantities are given by Nix (1964) as

$$V_1^{\text{CSE}}(\alpha) = {}^1E_c^0 \frac{\alpha^{2/3}}{2(1-\alpha^2)^{1/2}} \log\left[\frac{1+(1-\alpha^2)^{1/2}}{1-(1-\alpha^2)^{1/2}}\right] \quad \text{prolate } \alpha < 1,$$

$$= {}^1E_c^0 \alpha^{2/3} \frac{\tan^{-1}(\alpha^2-1)^{1/2}}{(\alpha^2-1)^{1/2}} \quad \text{oblate } \alpha > 1,$$

$$= {}^1E_c^0 = \tfrac{3}{5} Z^2 e^2/R_1 \quad \text{sphere } \alpha = 1,$$

$$V_1^{\text{SSE}}(\alpha) = {}^1E_s^0 \alpha^{2/3}\left[1 + \frac{\sin^{-1}(1-\alpha^2)^{1/2}}{\alpha(1-\alpha^2)^{1/2}}\right] \quad \text{prolate } \alpha < 1,$$

$$= {}^1E_s^0 \frac{\alpha^{2/3}}{2}\left[1 + \frac{\log(\alpha^2-1)^{1/2} + \alpha}{\alpha(\alpha^2-1)^{1/2}}\right] \quad \text{oblate } \alpha > 1,$$

$$= {}^1E_s^0 = a_s(1 - KI^2)A_1^{2/3} \quad \text{sphere } \alpha = 1.$$

Subscript and superscript 1 refers to nucleus 1. ${}^1E_c^0$ and ${}^1E_s^0$ are the SCE and SSE of the spherical nucleus 1. The surface energy parameter $a_s = 17{\cdot}9439$ MeV, the surface energy constant $K = 27{\cdot}9198/15{\cdot}4941$ and the neutron asymmetry term $I = (N_i - Z_i)/A_i$, N_i, Z_i and A_i being neutron, proton and mass number of the nucleus.

2.5 *Fusion cross-section*

The asymptotic de Broglie wavelength ($\lambda\!\!\!^{-}$ at ∞) is small compared to the dimension of the colliding nuclei even for light colliding systems. For a light system like ^{24}Mg + ^{24}Mg above coulomb barrier V_{CB} (= 22 MeV) at $E_{cm} = 24{\cdot}7$ MeV, $\lambda\!\!\!^{-}_\infty = 0{\cdot}26$ fm whereas the dimension of the colliding nuclei $R_1 + R_2 = 7$ fm. With increase in incident energy $\lambda\!\!\!^{-}_\infty$ decreases. So classical mechanics is expected to work well to describe ion-ion collision phenomena even for light systems. So the motion of the projectile can be described in terms of impact parameter or angular momentum. Using a sharp cut-off approximation the fusion cross-section σ_{CF} is given as

$$\sigma_{CF} = \pi \lambda\!\!\!^{-2}_\infty (l_{cr} + 1)^2$$

where the critical angular momentum $L_{cr} = l_{cr}\hbar$ corresponds to that trajectory at and below which all trajectories lead to fusion. Often σ_{CF} is taken to be

$$\sigma_{CF} = \pi\lambda\!\!\!^{-2}_{\infty} l^2_{cr}.$$

In our calculation we use

$$\sigma_{CF} = \pi\lambda\!\!\!^{-2}_{\infty} (l_{cr} + \tfrac{1}{2})^2. \tag{21}$$

Galin *et al* (1974) proposed a model called the critical distance approach model to describe fusion characteristics. According to this model if the projectile reaches a certain distance R_{cr} (critical distance) from the target, then it will be captured leading to fusion. In this model the expression for fusion cross-section σ_{CF} is

$$\sigma_{CF} = \pi R^2_{cr}\left(1 - \frac{V_{cr}}{E_{cm}}\right). \tag{22}$$

This formula of Galin *et al* (1974) was suitable for high energy fusion data. Gutbrod *et al* (1973) also used a somewhat similar formula to describe low energy fusion data as

$$\sigma_{CF} = \pi R^2_B\left(1 - \frac{V_{CB}}{E_{cm}}\right), \tag{23}$$

where R_B is the coulomb barrier radius and V_{CB} is the coulomb barrier. Glas and Mosel (1975) had tried to reconcile these two seemingly different formulae which refer to two different regions of energy. The plot of σ_{CF} *vs* E^{-1}_{cm} should have two straight lines of different slopes with a bend in between. Most of the experimental fusion cross-section data show the two-slope behaviour which is a very important feature of the capture process.

2.6 *Calculation of potentials for lighter systems*

The nuclear interaction potentials $V_N(r, \alpha)$ for six lighter pairs of nuclei have been calculated using the shape-dependent generalised single folding method of (16). These potentials were calculated at different deformations starting from $\alpha = 0{\cdot}62$ to $\alpha = 1{\cdot}24$ at intervals of 0·02 for r ranging roughly from 2 fm $< (R_{1D} + R_{2D})$ to about 18 fm at regular intervals of 0·5 fm. For example, for (Cl + Sn) system, we have generated the nuclear interaction potential V_N for $\alpha = 0{\cdot}62, 0{\cdot}64, 0{\cdot}66 \ldots 1, 1{\cdot}02, 1{\cdot}04, \ldots 1{\cdot}20, 1{\cdot}22, 1{\cdot}24$ and for each α the nuclear interaction potential V_N is calculated for $r = 7, 7{\cdot}5, 8 \ldots 12, 12{\cdot}5 \ldots 17{\cdot}5$ and 18 fm for 23 values of r at regular intervals of 0·5 fm. The potentials at a given α and all r have been fitted into a polynomial form

$$V_N(r, \alpha) = -\sum_{n=1}^{5} A_n(\alpha)(r - R)^{n-1} \log\left[1 + \exp\left(-\frac{r - R}{a(\alpha)}\right)\right], \tag{24}$$

where $R = 1{\cdot}3(A_1^{1/3} + A_2^{1/3})$, A_i being masses of the projectile and target. For potential V_N at each deformation α, we vary the diffuseness coefficient a till we get the best fit. Thus for each α, we get a fixed diffuseness coefficient a and a set of polynomial coefficients A_1, A_2, A_3, A_4 and A_5. Therefore A_n's and a's are α dependent. The nuclear interaction potentials at a given deformation as a function of r are presented in figures 2–4.

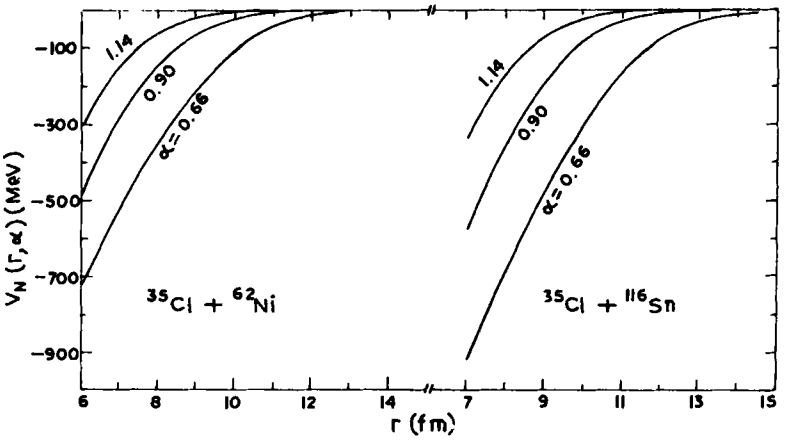

Figure 2. The nuclear interaction potential energy V_N vs r for different deformations.

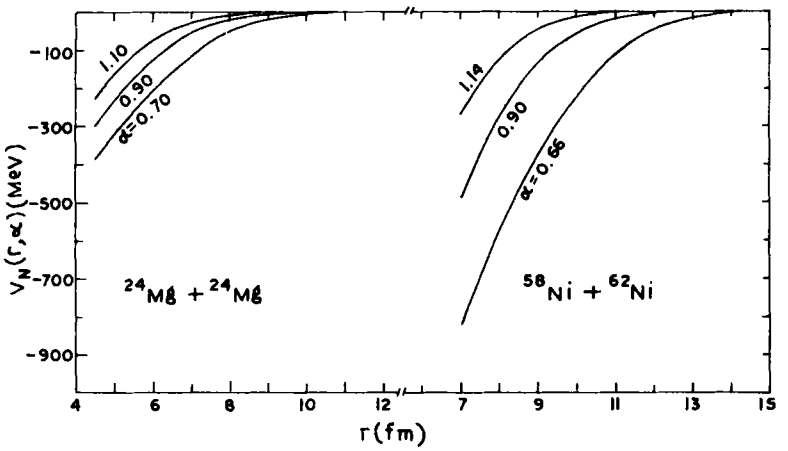

Figure 3. Same as figure 2.

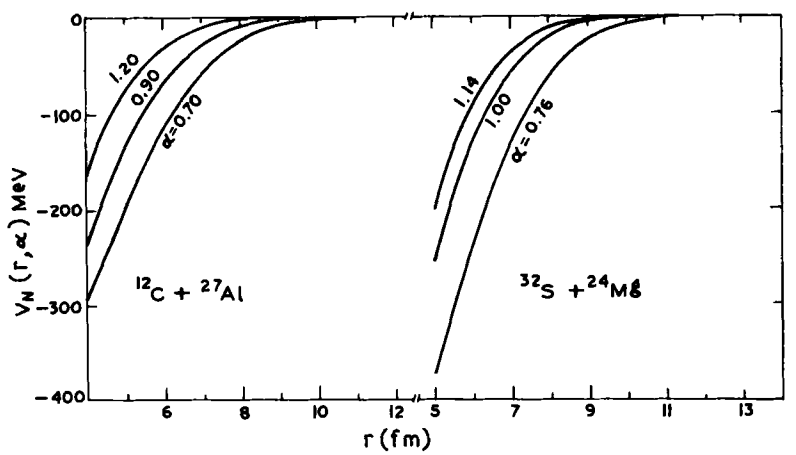

Figure 4. Same as figure 2.

3. Results and discussion

We have calculated the nuclear interaction potential V_N as a function of inter-nuclear separation r and deformation α for six lighter systems using the generalised folding method. It is often argued that the folding model gives nuclear potentials which are unrealistic at short distances. It is true that folding potentials are too attractive and do not adhere to Pauli and other correlation effects properly. But for low and medium energy heavy ion interactions, only the tail region of the potential is relevant. Therefore it is irrelevant how deep it is beyond the interaction region. In the interaction region, it is neither too deep nor too shallow. Also it is interesting to note that for a given system as the nuclei become more and more elongated (prolate shapes with α decreasing from 1), the range of the nuclear potential (the inter-nuclear separation distance for which V_N goes to zero) increases. This point can be seen from figures 2–4. This is expected since the proximity of the two nuclei increases as the nuclei becomes more and more prolate. Also for different systems at same r and α, the nuclear interaction potentials are different, the heavier the system, the deeper is the potential. This is expected since for same r and α, for the heavier system there will be more density overlap than the lighter ones. This can also be seen from figures 2–4. It is found that at $r = 10$ fm and $\alpha = 0{\cdot}80$, the nuclear interaction potential

$$V_N = -3{\cdot}21 \text{ MeV} \quad \text{for } {}^{24}\text{Mg} + {}^{24}\text{Mg},$$

$$V_N = -98{\cdot}30 \text{ MeV} \quad \text{for } {}^{58}\text{Ni} + {}^{62}\text{Ni},$$

$$V_N = -139{\cdot}89 \text{ MeV} \quad \text{for } {}^{35}\text{Cl} + {}^{116}\text{Sn}.$$

On applying our deformation model to lighter systems we find that an appreciable oblate deformation is obtained at closest approach contrary to the assumptions of spherical shape in entrance channel of Wilczynska *et al* (1976). For C + Al we find that at $E_{lab} = 180$ MeV for $L = 33$, the oblate deformation at closest approach is 1·19. Similarly for Cl + Sn it is 1·21 at $E_{lab} = 439{\cdot}8$ MeV for $L = 107$, 1·11 for $L = 69$ for Cl + Ni at $E_{lab} = 225{\cdot}6$ MeV, 1·18 for $L = 91$ for Ni + Ni at $E_{lab} = 449$ MeV, 1·116 for $L = 45$ for S + Mg at $E_{lab} = 233$ MeV and 1·116 for $L = 40$ for Mg + Mg at $E_{lab} = 179{\cdot}4$ MeV.

In the actual calculation, we take a particular pair of nuclei at a given energy above coulomb barrier and solve (5), (6) and (7) for r, θ and α degrees of freedom for a given L using the Runge-Kutta (RK) method. Initially we start with two spherical nuclei ($\alpha = 1$) with r of about 18 fm such that the nuclear interaction is effectively zero. The initial θ is supplied using Rutherford's well-known formula connecting r, θ and the eccentricity of the orbit. Initial $\dot{\theta} = L/\mu r^2$, initial $\dot{\alpha}$ is taken to be zero and initial $\dot{r}$ is obtained by equating the initial centre of mass energy E_{cm} with the kinetic and the potential energies at the starting point. Quantities like $r, \dot{r}, \theta, \dot{\theta}, \alpha, \dot{\alpha}$ at subsequent stages are obtained by the RK method. The deformation changes from the initial spherical shape to the oblate shape due to coulomb repulsion and strong surface friction in the entrance phase (velocity decreases almost to zero) and after closest approach velocity becomes positive, the shape changing from oblate to less oblate, spherical and finally to prolate. If the trajectory at a given L in question is obtained after some energy loss, we take the event to be an inelastic collision but if for a smaller L, we find that the trajectory does not have anything like a closest approach, the internuclear separation r steadily goes on decreasing, the velocity continues to decrease, we assume that the two nuclei have a

tendency for fusion. The highest L for which the trapping occurs and the projectile is unable to come out is taken to be the critical angular momentum L_{cr} of the system at the given energy. All trajectories at a given energy below this L_{cr} are trapped, contributing to fusion. So after locating L_{cr}, we theoretically calculate fusion cross-section σ_{CF} using (21). Energy dependence of the system is studied by going over to different incident energies above coulomb barrier. Using different L, L_{cr} is located and σ_{CF} is again calculated using the new L_{cr} and the new E_{cm} of the system.

We have compared our nuclear interaction potential obtained from single folding calculation with the potential obtained from elastic scattering data in figure 4a for $^{24}Mg + ^{24}Mg$. The real part of the optical potential having W-Saxon form is

$$V_N = \frac{V}{1 + \exp\left(\frac{r-R}{a}\right)}$$

where $V = 2{\cdot}9$ MeV, $a = 0{\cdot}58$ fm and $R = 8{\cdot}65$ fm as given by Jachcinski *et al* (1981) obtained from a fitting with elastic scattering data. Using the experimental fusion data they have extracted coulomb barrier $V_{CB} = 22{\cdot}3 \pm 0{\cdot}4$ MeV and barrier radius $R_B = 8{\cdot}9 \pm 0{\cdot}3$ fm. After crossing R_B a trajectory is likely to be trapped. So a separation distance $8{\cdot}9 < r < 11$ fm or so is the relevant region of interaction where the magnitude of the two potentials can be compared. As seen from figure 4a for $^{24}Mg + ^{24}Mg$ at $r = 9, 9{\cdot}5, 10, 10{\cdot}5, 11$ fm $V_N = -(3{\cdot}7, 1{\cdot}95, 1, 0{\cdot}5, 0{\cdot}25)$ MeV from single folding calculation for spherical nuclei and $V_N = -(1, 0{\cdot}5, 0{\cdot}28, 0{\cdot}12, 0{\cdot}05)$ MeV respectively from optical model fitting of elastic scattering data. Therefore, although the difference widens at

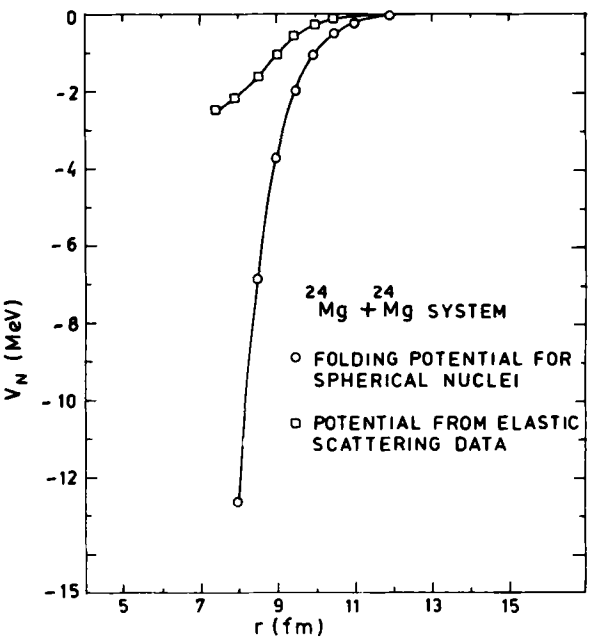

Figure 4a. Comparison of single folding nuclear interaction potential for $^{24}Mg + ^{24}Mg$ for spherical case with the potential obtained from elastic scattering data.

short distances for these two potentials, yet in the region of interest they fairly agree. That is why it matters little though the forms of the two potentials differ drastically at short distances.

The two-slope-behaviour of fusion systematics is well understood theoretically and is observed experimentally in a number of systems that have been thoroughly investigated at a wide range of energies. As shown in (21), fusion cross-section depends on l_{cr}^2/E_{cm} for a particular pair of nuclei. At low incident energies above the s wave barrier, the fusion cross-section increases with energy because higher L potential pockets are explored and l_{cr}^2 becomes the dominant term. But as we go to higher L, the potential energy pockets become more shallow due to the centrifugal term and finally the pockets disappear completely. Though increase in E_{cm} helps the projectile in seeing a higher L pocket, thereby increasing L_{cr} and hence σ_{CF}, yet after the pockets disappear, there is no guarantee that the projectile could be trapped. Even though we are free to increase E_{cm} indefinitely, we cannot increase l_{cr} without limit. For a particular pair of nuclei, the l_{cr} approaches a saturation value which limits the numerator of (21). Again in the denominator occurs E_{cm}, the increased value of which pulls σ_{CF} down. So σ_{CF} is bound to decrease at high energies. This clearly explains the increase of σ_{CF} initially and decrease of σ_{CF} at very high energies through a bend. The increase of σ_{CF} in the initial stage is very fast because for a small energy above the barrier, many partial waves contribute to fusion but at high energy decrease of σ_{CF} is rather gradual as L_{cr} becomes almost steady and E_{cm} term in the denominator of (21) slowly dominates over the numerator.

We have presented the fusion cross-sections obtained in our model calculation in figures 5–10. The increase of fusion cross-section initially above the coulomb barrier energy and its decrease at very high energies, giving a two-slope behaviour of fusion

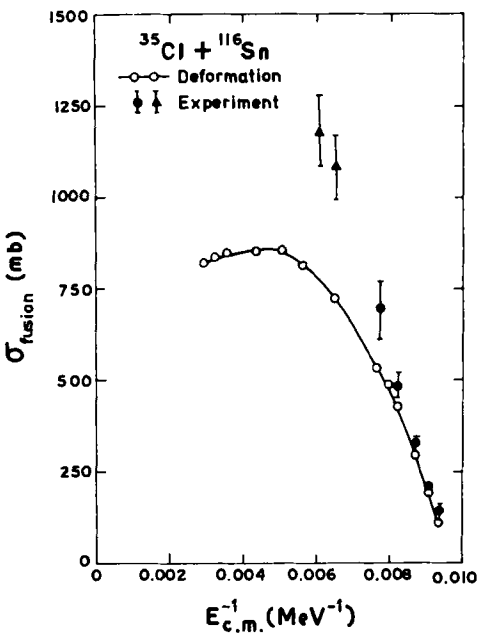

Figure 5. Fusion cross-section σ_{CF} *vs* E_{cm}^{-1}.

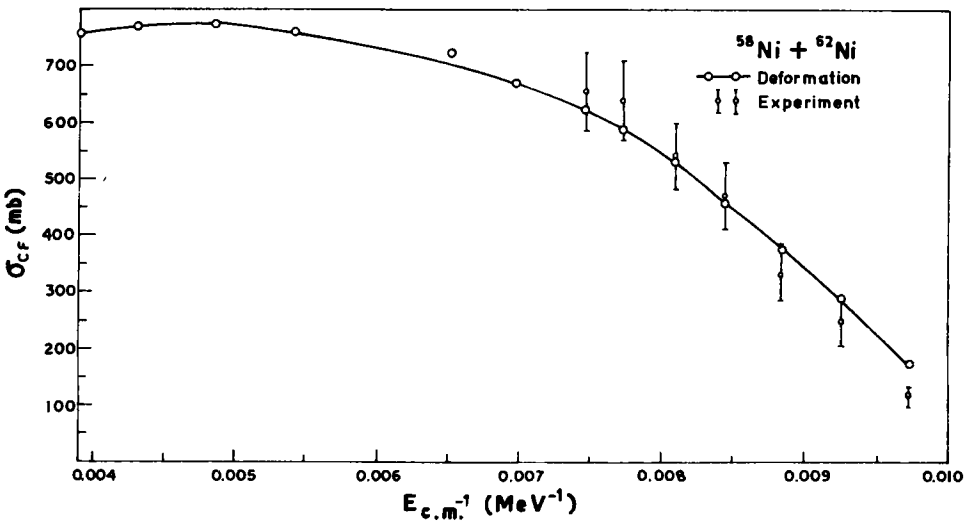

Figure 6. Same as figure 5.

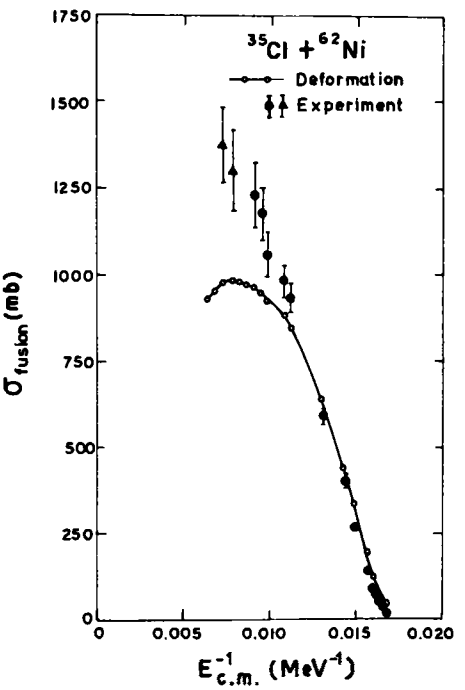

Figure 7. Same as figure 5.

cross-section with a bend in between, have been obtained in our calculation. For all the systems studied by us, we find that for initial increase of incident energy above the coulomb barrier, increase of σ_{CF} is very fast but at higher energies, its decrease is very gradual. To know fusion systematics correctly, it is essential that a system must be thoroughly studied. At present, data are inadequate in certain cases. $^{12}C + ^{27}Al$ has

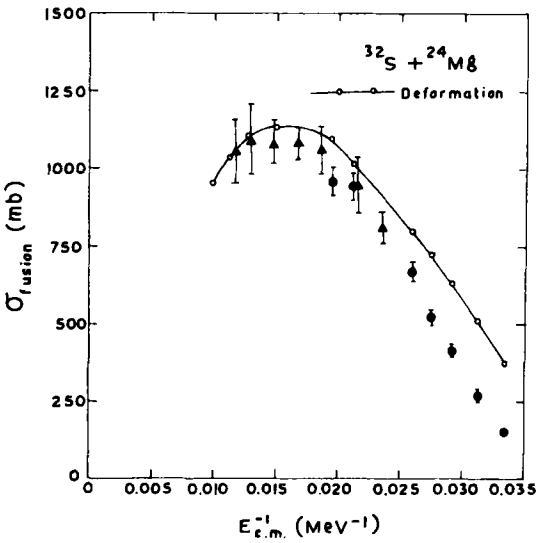

Figure 8. Same as figure 5.

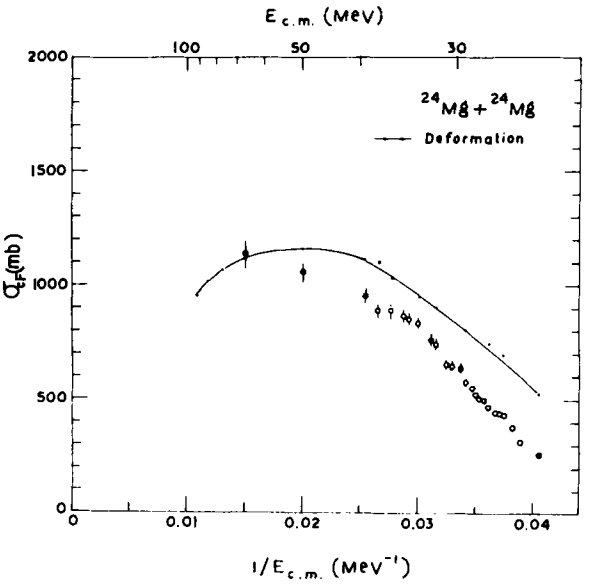

Figure 9. Same as figure 5.

been experimentally investigated thoroughly. The two-slope-behaviour and a bend at intermediate energy has been obtained experimentally. Our model calculations for this system agree well with experiment (figure 10). For the $^{32}S + ^{24}Mg$ system (figure 8) our results agree fairly with experiment. Experimental data are inadequate as the experiment has not been extended to very high energies, yet the trend for decrease of σ_{CF} with increase of energy is well indicated. We have obtained the two-slope-behaviour in this case. Jachcinski *et al* (1981) studied $^{24}Mg + ^{24}Mg$ experimentally but the system

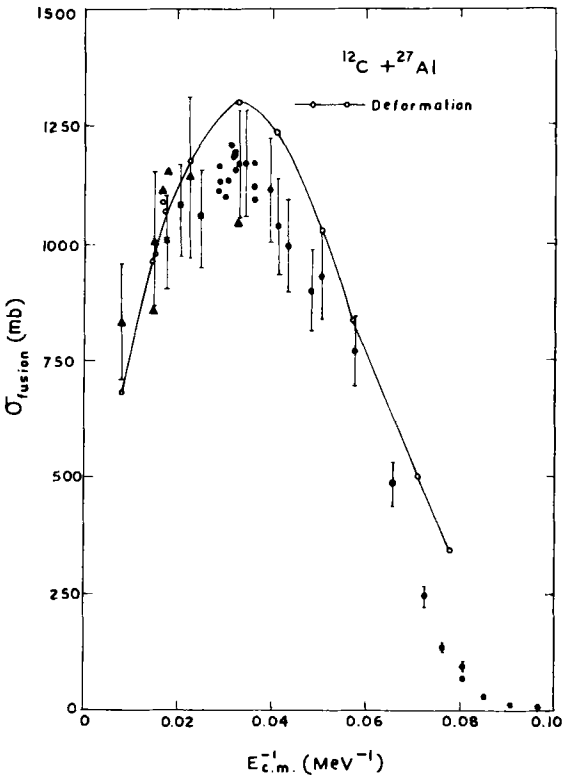

Figure 10. Same as figure 5.

has not been investigated at high energies. In our model calculation we have obtained the two-slope-behaviour and the overall agreement with experiment is fairly good (figure 9). Sikora *et al* (1982) have experimentally investigated the $^{58}Ni + ^{62}Ni$ system. For this system our result agrees quite well with experiment and we have obtained the two-slope behaviour (figure 6).

In $^{35}Cl + ^{116}Sn$ (figure 5) and $^{35}Cl + ^{62}Ni$ (figure 7) systems our fusion systematics show the two-slope behaviour with a bend in between. The initial increase of σ_{CF} with energy and the decrease of σ_{CF} at high energies have also come up in our model calculations. Our fusion cross-sections fairly agree with experiment only at low energies in these two cases. But at high energies the disagreement is more pronounced. One of the reasons for this could be that the experimental fusion cross-sections are a little overestimated. Scobel *et al* (1976) admitted that the fission fragments which they have included as arising from fusion might have arisen from asymmetric fission of inelastic origin. So the experimental σ_{CF} reported by them might be a little higher than the actual σ_{CF}. The other reason is that in our model the oblate shape at closest approach enhances the coulomb barrier resulting in reduction of L_{cr} and hence reduction of σ_{CF}. Experimentally the two-slope behaviour is not exhibited for $^{35}Cl + ^{62}Ni$, $^{35}Cl + ^{116}Sn$ and $^{58}Ni + ^{62}Ni$. Two-slope behaviour is a very well-known feature of fusion systematics but unless the systems are extensively studied at a wide range of energies, we cannot hope to get such a feature.

An interesting outcome of the study of fusion systematics of light ions is the observation of structures or periodic oscillations in the energy dependence of fusion cross-sections. Now the oscillatory nature of fusion excitation functions of some light systems like $^{12}C+^{12}C$, $^{12}C+^{24}Mg$, $^{12}C+^{16}O$ and $^{16}O+^{16}O$ is surprising. Again absence of such structures for some neighbouring interacting nuclei is also surprising. The presence and absence of oscillations in fusion cross-sections in some systems reflects the role of the clusters present in the nuclei. $^{24}Mg+^{24}Mg$ system was studied experimentally by Jachcinski *et al* (1981) with such a perspective. They found a structureless fusion cross-section increasing with incident energy above the barrier in line with Gutbrod *et al* (1973) and Glas and Mosel (1975) at low energies. No oscillation is observed in fusion cross-section. Since it has not been studied at high energies experimentally, Jachcinski *et al* (1981) have not been able to provide the nature of the curve at high energies. We have theoretically studied the system at high energies and have obtained decrease of fusion cross-section at high energies and an intermediate bend in line with predictions of Glas and Mosel (1975).

4. Conclusion

We have developed a classical friction model for the scattering of deformed nuclei to describe capture processes for comparatively lighter heavy ions. We have incorporated the spheroidal deformation dynamically into our model. In ion-ion collision Birkelund *et al* (1979) use the well-known expression for reduced mass even up to a separation distance of 0·2 fm which is not justified. But in our model the half density surface separation is greater than 2 fm even for most penetrating trajectories. So the two-body dynamics remains clean throughout the entire collision process.

We find that the two-slope behaviour of fusion systematics is well reproduced in our model. For $^{58}Ni+^{62}Ni$ our model gives fusion cross-sections well within the experimental uncertainties. For $^{24}Mg+^{24}Mg$ at low energies, our capture cross-sections differ significantly from experiment. Gross and Satpathy (1981, 1982) and Satpathy (1982) have also noticed similar overshooting of capture cross-sections for light ions at low energies. They argue that the density profile for a heavy system and a light system cannot be similar. For light systems they have modified the strength of W-Saxon potential to $V_0 = -40$ MeV and diffuseness coefficient to $a_p = 0{\cdot}45$ fm from $V_0 = -50$ MeV and $a_p = 0{\cdot}65$ fm. This agrees with experiment.

Acknowledgements

The author is grateful to Prof. L. Satpathy for his interest in the work, for discussions with him and for a critical reading of the manuscript. He is thankful to Prof. D H E Gross (Berlin) for past useful communications.

References

Birkelund J R, Tubbs L E, Huizenga J R, De J N and Sperber D 1979 *Phys. Rep.* **56** 107
Deubler H H and Dietrich K 1977 *Nucl. Phys.* **A277** 493
Galin J, Guerreau D, Lefort M and Tarrago X 1974 *Phys. Rev.* **C9** 1018

Glas D and Mosel U 1975 *Nucl. Phys.* **A237** 429
Gross D H E, Kalinowski H and De J N 1974 *Lect. Notes* **33** 194
Gross D H E and Satpathy L 1981 *Int. Workshop Nucl. Phys.* (ICTP) Trieste
Gross D H E and Satpathy L 1982 *Phys. Lett.* **B110** 31
Gross D H E, Nayak R C and Satpathy L 1981 *Z. Phys.* **A299** 63
Gutbrod H H, Winn W G and Blann M 1973 *Nucl. Phys.* **A213** 267
Hirschfelder J O, Curtiss C F and Bird R B 1954 *Molecular theory of gases and liquids* (New York: John Wiley) 835
Jachcinski C M, Kovar D G, Betts R R, Davids C N, Geesaman D F, Olmer C, Paul M, Sanders S J and Yntema J L 1981 *Phys. Rev.* **C24** 2070
Nayak R C 1983 *Deep inelastic collision of heavy ions*, Ph.D. thesis (unpublished) Utkal University (India)
Nix J R 1964 Lawrence Radiation Laboratory, Berkeley Report UCRL 11338 178
Satpathy L 1982 *Proc. Second Indo-US Symp. Nucl. Phys. at Cyclotron and Intermediate energy*, Bombay
Scobel W, Gutbrod H H, Blann M and Mignerey A 1976 *Phys. Rev.* **C14** 1808
Sikora B, Blann M, Scobel W, Bisplinghoff J and Beckerman M 1982 *Phys. Rev.* **C25** 885
Wilczynska K S and Wilczynski J 1976 *Nucl. Phys.* **A264** 115